Ceramics-Silikáty 65 (3), 295-304 (2021)
www.ceramics-silikaty.cz doi: 10.13168/cs.2021.0031

EXPERIMENTAL INVESTIGATION AND NON-LOCAL MODELLING OF THE THERMOMECHANICAL BEHAVIOUR OF REFRACTORY CONCRETE

#BELGACEM MAMEN*, FAROUK BENALI**, ABDELAZIZ BOUTRID***, ****, MOHAMED SAHLI*****, MOHAMED HAMIDOUCHE******, GILBERT FANTOZZI*******

*Department of Civil Engineering, Abbès Laghrour University, Khenchela 40000, Algeria
**Laboratory of Non-Metallic Materials, Ferhat Abbas University Setif 1, Sétif 19000, Algeria
***Department of Civil Engineering, Abbès Laghrour University, Khenchela 40000, Algeria
****Mineral Processing and Environmental Laboratory, Department of Mines, Badji Mokhtar University, Annaba 23000, Algeria
*****EMTO-ST Institute, CNRS/UFC/ENSMM/UTBM, Department of Applied Mechanics, Université Bourgogne Franche-Comté, 25000 Besancon, France
******Emergent Materials Research Unit, Université Ferhat Abbas Sétif 1, Sétif 19000, Algeria
*******University of Lyon, INSA-Lyon, MATEIS CNRS-UMR5510, 69621 Villeurbanne, France

#E-mail: belgacem.mamen@univ-khenchela.dz

Submitted June 10, 2021; accepted August 16, 2021

Keywords: Silica-alumina refractory concrete, High temperatures, Cracking propagation, Nonlocal finite element model

This paper describes an experimental characterisation and a non-local finite element analysis on the influence of the testing temperature on the mechanical properties and cracking propagation in refractory cement bricks. Therefore, isothermal four-point bending and uniaxial compression tests have been carried out at different testing temperatures (25, 500, 800, and 1000 °C) to determine the stress-strain response for each independent testing temperature. Based on this response, material constants are identified using the inverse estimation method. Then, they are introduced in a non-local finite element model using CAST3M software. The experimental results indicate that with an increase in the testing temperature, the thermomechanical behaviour of the refractory concrete shows a critical temperature of 800 °C, for which the compression and tensile strengths are the largest. Their values are respectively around 28 and 9 MPa. The present numerical simulation results indicate two types of crack propagation; continuous crack failures when the temperature varies between 25 and 800 °C and multi-identified cracks producing a localised damage zone at 1000 °C. Notably, the sample tested at 1000 °C requires a deflection of 0.2 mm to achieve 0.3 (30 % damaged). In contrast, the damage variable achieves 1.0 (100 % in damage) for the sample tested at 25 °C with the same imposed displacement (0.2 mm). Finally, the enhanced non-local damage model produces a realistic simulation of the experimental failure mechanisms, proving the validity of the implementation method.

INTRODUCTION

Refractory concretes are the simplest to implement among monolithic refractories. They are generally composed of a mixture of refractory cement and aggregates in addition to small amounts of some other elements like silica fume to improve other chemical and physical properties [1–6]. For the last 20 years, refractory concrete has improved to be relatively easier to use than shaped materials. Moreover, it is commonly used in various installations where severe coupled thermal stresses and mechanical loadings are applied: cement furnaces, electric arc furnaces and blast furnaces [7, 8].

Many researchers have studied the mechanical properties of refractory concretes at room temperature through tension, bending, and compression tests. Schmitt et al. determined Young's modulus and the tensile properties of two industrial refractories using uniaxial tension and three-point bending tests. They concluded that the Young's modulus derived from both tests is nearly the same [9]. Additionally, Simonin et al. conducted four-bending tests on aluminous refractory concretes fired at different temperatures ranging from 200 to 1600 °C. Strain gauges were set on the tensile and compressive surfaces to measure the relative difference in the elastic modulus. They concluded that the relative difference is minimal for the samples fired at 450 °C or below. Above this temperature, the difference in the modulus sharply increases [10]. Also, Kakroudi et al. investigated the mechanical properties of two refractory castables fired at different temperatures ranging from 110 to 1100 °C using tensile tests. They found that the damage behaviour is typically associated with the firing temperature in both castables [2]. High temperatures are described as one of the most critical physical deterioration procedures that affect the quality and sturdiness of concrete structures [11]. However, very few researchers have focused on identifying and understanding the thermo-mechanical behaviour of refractory concretes.

Aksel investigated the mechanical properties and thermal shock behaviour of slip-cast alumina-mullite refractories by incorporating fine-grain alumina and mullite particles. Both the densification and mechanical properties considerably increased with the addition of alumina particles compared to mullite. Also, when increasing quench temperature, the strength and Young's modulus were improved, leading to high thermal shock resistance [12]. Boussuge analysed the thermomechanical properties of two industrial refractories: fused-cast materials and alumina castables. Based on the tension, compression and bending tests, both materials exhibit creep at high temperatures. Also, the macroscopic viscoplasticity has been studied by analysing the microstructural mechanisms of the deformation. In addition, they pointed out that the thermo-mechanical behaviour of the castables was greatly influenced by the nature and the adhesion of the aggregates [13]. Amrane et al. carried out compression and three-point bending tests to highlight the thermo-mechanical behaviour of refractory products made from Algerian refractory clays. All the tests were undertaken at temperatures between 25 °C and 1200 °C. It was reported that between room temperature and 900 °C, the mechanical behaviour was quasi-brittle. Above this temperature, the refractory material exhibited only viscous behaviour [14]. Another study by Benali et al. shows that the difference in the thermal expansion between the refractory concrete constituents can significantly affect its thermo-mechanical behaviour. Additionally, the differential expansions of the numerous phases are the primary source of the presence of various microcracks [14]. More importantly, these microcracks may cause a reduction in the material's capacity to resist externally applied forces. In this regard, the continuum damage mechanics considers the damage indirectly through an internal variable.

Different models define this internal parameter as a scalar [15, 16] or tonsorial variable [17, 18], while other models have two independent damage variables, one for tensile damage and another for compressive damage [19–21]. However, only a limited amount of work has studied the modelling of the thermomechanical behaviour of refractory materials and the damage evolution [8, 22, 23].

To improve the knowledge of the thermomechanical behaviour of refractory materials during the service life of cement furnaces, isothermal four-point bending and uniaxial compression tests were performed in the present study using different testing temperatures (25, 500, 800 and 1000 °C). Based on the experimental tests, the material constants were identified using the inverse estimation method. Then, they were introduced in an enhanced non-local damage model using CAST3M software. Finally, the main concern is to find out the effect of temperature on the mechanical properties and cracking propagation in refractory cement bricks.

EXPERIMENTAL

Materials and sample preparation

Two commercial products were considered for the elaboration of the silica-alumina refractory concrete. The first product is an anhydrous mortar (CH45) made of fused cement from Kernos (France) and Andalusite mineral waste residue. The second is DD3 kaolin extracted from Djebbel Debbagh, Algeria. The DD3 kaolin is used in crude and calcined forms (Chamotte). The chemical compositions of CH45 and DD3 were systematically investigated by an X-ray fluorescence spectrometer and are summarised in Table 1. As shown in Table 1, both products are relatively high in alumina (46.70 and 38.36 wt. %), suitable for manufacturing shaped refractories [24]. The raw material content and the granulometry of each component used to elaborate the silica-alumina refractory concrete are summarised in Table 2.

The present refractory material was prepared by mixing the raw materials with an adequate amount of distilled water (18.7 wt. % of the dry content) according to the standard "Ball-In Hand Test" ASTM C860-15 (2019) [25]. The mixed slurry was cast into moulds of

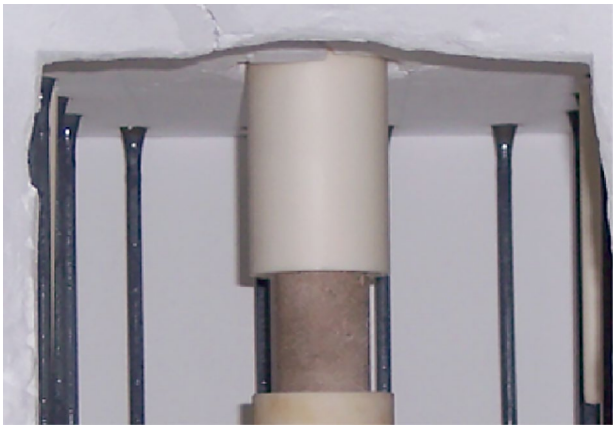

a)

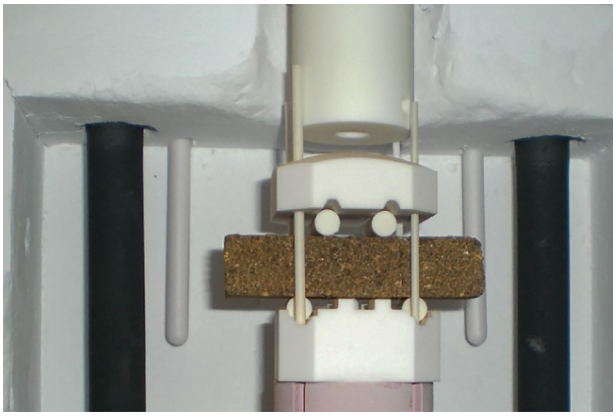

b)

Figure 1. Refractory concrete samples used for: a) uniaxial compression test; b) four-point bending test.

150 × 30 × 30 mm for the bending tests and 30 mm diameter cylindrical moulds with 50 mm in height for the uniaxial compression tests, see Figure 1. Then, the samples were incubated for 24 h at 25 °C with 98 % relative humidity before demoulding. Immediately after demoulding, the samples were submerged under water for about three days, followed by drying at 110 °C for 24 h. Finally, the firing step was made at 1450 °C in an electric furnace for two hours.

Table 1. Chemical composition of the anhydrous mortar (CH45) and calcined kaolin (DD3).

Elements (wt. %)	Anhydrous mortar (CH45)	Kaolin (DD3)
SiO_2	35.42	39.87
Al_2O_3	46.70	38.36
Fe_2O_3	1.29	1.14
CaO	10.15	0.78
Na_2O	0.20	0.48
MnO	–	0.46
SO_3	–	0.45
MgO	0.42	0.24
K_2O	0.78	0.20
P_2O5	–	0.02
TiO_2	–	0.02
Cr_2O_3	0.17	0.01
ZrO_2	0.35	–
Calc. loss	4.52	17.27

Table 2. Raw materials in (wt. %) of the silico-alumina refractory concrete.

Raw materials	Grain size	(wt. %)
Anhydrous mortar (CH45)	Fused cement: $\Phi \leq 0.4$ µm	7
	Andalusite: $\Phi \leq 0.2$ mm	38
Calcined kaolin (DD3)	DD3 (fine): $0.135 \leq \Phi \leq 1.25$ mm	10
	DD3 (large): $1.6 \leq \Phi \leq 3.5$ mm	45

Thermomechanical testing procedure

At this level, the thermomechanical behaviour of the refractory concrete is characterised up to 1000 °C using an MTS 30/ml electromechanical testing machine.

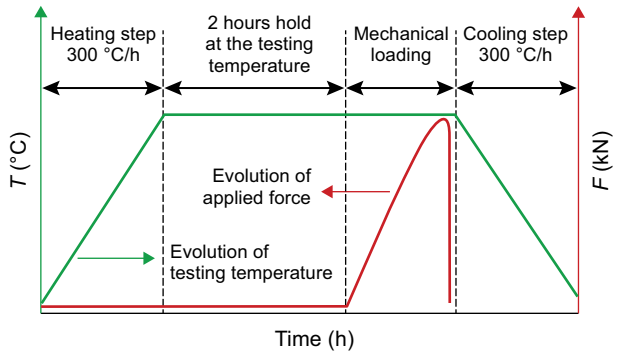

Figure 2. Schematic illustration of the thermomechanical testing procedure.

The thermomechanical characterisation is conducted according to the schematic illustration presented in Figure 2. First, the samples were heated to the testing temperature at a heating rate of 300 °C·h^{-1}, followed by holding for two hours at the same testing temperature. Then, a mechanical load was applied in isothermal conditions. Finally, the samples were slowly cooled to room temperature.

COMPUTATIONAL METHODS

Nonlocal damage model

The present model is characterised by a regularisation considering a lower mesh size dependency [26]. The general behaviour law relating the Cauchy stress tensor σ to the strain tensor ε is given as follows:

$$\sigma = (1 - D)\, E : \varepsilon \tag{1}$$

where E is the undamaged stiffness and D is the isotropic damage variable increasing from 0 for the virgin material to 1 for the completely damaged material.

It is assumed that D depends on a state variable Y.

The non-local regularisation method has been used to replace the state variable Y by its non-local counterpart $\tilde{Y}$ following Equation 2, [27].

$$\tilde{Y} = \frac{\int_V \alpha\,(d)\; Y\, dV}{\int_V \alpha\,(d)\, dV} \tag{2}$$

where α is a Gaussian function given as follows:

$$\alpha\,(d) = \exp\left[-\left(\frac{2d}{l_c}\right)^2\right] \tag{3}$$

where l_c is a material parameter of the non-local damage model called the characteristic length and Y is the state variable, which drives the damage $D = D(\tilde{Y})$ according to Mazars law [28]:

$$Y = \sqrt{\sum_i [\max\,(0, \varepsilon_i)]^2} \tag{4}$$

In this case, the damage variable is controlled by the tensile portion D_t and the compressive portion D_c.

$$D = \alpha_t^{\beta}\, D_t + \alpha_c^{\beta}\, D_c \tag{5}$$

where α_t and α_c are the associated Gaussian functions and β is the constant related shear behaviour. The damage parts D_t and D_c are given as follows:

$$D_{t,c} = 1 - \frac{Y_{D0}\,(1 - A_{t,c})}{Y} - \frac{A_{t,c}}{\exp\,[B_{t,c}\,(Y - Y_{D0})]} \tag{6}$$

where Y_{D0}, A_t, B_t, A_c and B_c are the material constants of the Mazars' damage model.

By applying the non-local stress based (NLSB) [26], the Gaussian function becomes as follows:

$$\alpha(d) = \exp\left[\left(\frac{2d}{l_c \cdot \rho}\right)^2\right] \quad (7)$$

where ρ is the stress factor.

Identification of model parameters

Based on the experimental stress-strain curves obtained from the uniaxial compression and four-point bending tests, the material constants describing the shape of the stress-strain curve were identified for each testing temperature using the inverse estimation method, see Equation 8. The selected refractory concrete is homogeneous isotropic and characterised by Young's modulus E. Its values are calculated based on the experimental compression stress-strain curves, see Figure 3a. The identified material constants of the stress-based nonlocal damage model for the different testing temperatures are summarised in Table 3.

$$\begin{cases} \min G(x) \\ G(x) = \sum_i^n \left|\sigma_{\exp}(\varepsilon_i, x) - \sigma_{num}(\varepsilon_i, x)\right|^2 \\ x = [A_c, B_c, A_t, B_t, Y_{D0}] \end{cases} \quad (8)$$

RESULTS AND DISCUTION

Effect of temperature on the thermomechanical behaviour of the refractory concrete

To analyse the effect of the temperature on the thermomechanical behaviour of the refractory concrete, uniaxial compression and four-point bending tests were carried out at 25, 600, 800 and 1000 °C. The associated stress-strain curves obtained by the uniaxial compression and four-point bending tests are shown in Figures 3a and 3b, respectively. These curves show an increase in the material strength with an increasing temperature till 800 °C. Beyond this temperature, the material strength decreases to a minimum value. Accordingly, the progress of the curves, see Figures 3a and 3b, demonstrates two behavioural trends. First, the tests performed at 25, 600 and 800 °C display a quasi-brittle behaviour where the curves are almost linear up to the maximum stress. After reaching the maximum value, the stress-strain curves suddenly fall; this is normally due to a brittle fracture. Second, at 1000 °C, the stress-strain curves have an open bell-shaped form and the material's ductility increases. More importantly, the bending strains developed by the refractory concrete at the peak stress are increased

Table 3. Model parameters for the silica-alumina refractory concrete.

Identified material constants	Testing temperatures			
	25 °C	600 °C	800 °C	1000 °C
Y_{D0}	2.0×10^{-5}	1.3×10^{-3}	1.1×10^{-4}	2.36×10^{-4}
A_t	1	1	0.7	0.93
B_t	19000	10000	500	300
A_c	2.90	1.09	2.47	1.71
B_c	896.84	616.16	451.03	327.10
B	1.06	1.06	1.06	1.06
l_c (cm)	2	2	2	2
E (GPa)	5313.5	4342.3	3984.4	1282.1

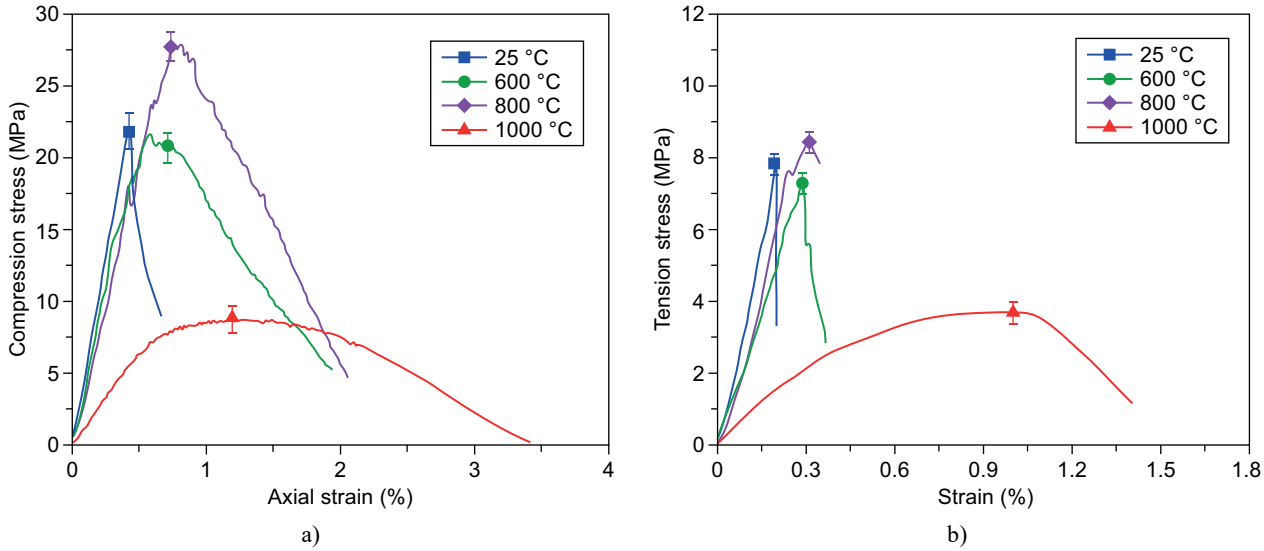

a) b)

Figure 3. Complete stress-strain curves for the silico-alumina refractory concrete tested under the different testing temperatures: a) uniaxial compression; b) four-point bending.

(1.0 - 1.1 % compared with 0.2 - 0.3 % at lower temperatures). Also, the stress level remains relatively constant over a large range of strain and then decreases slowly toward a significant deformation confirming the viscoplastic behaviour at this temperature.

Effect of temperature on the mechanical strength and strain

The refractory concrete's maximum mechanical strength and strain evolution is illustrated in Figures 4a and 4b for testing the temperature using two techniques: four-point bending and uniaxial compression tests. The recorded data are the average values of three tests at each temperature. The compressive strength and strain values are more significant than the bending strength and bending strain values; because refractory concrete, as a brittle material, generally has a higher compression strength than its tensile strength. Importantly, the maximal strength is attained at 800 °C. More importantly, the amorphous phase viscosity is enough to form bridges between different grains at this temperature. Therefore, this grain bridging process generates an increase in the compressive and flexural strengths.

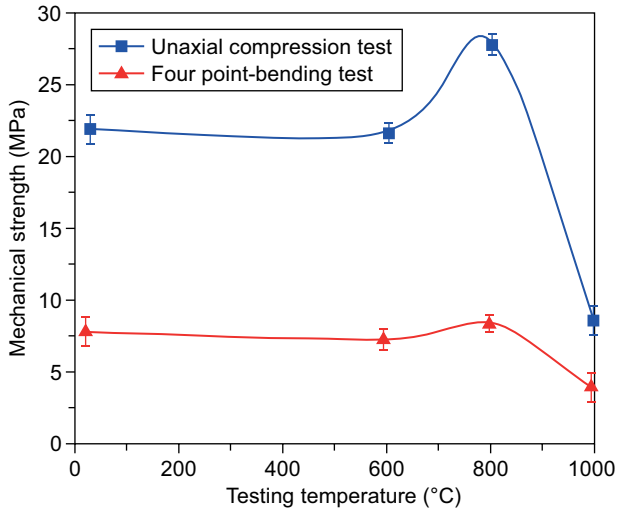

a)

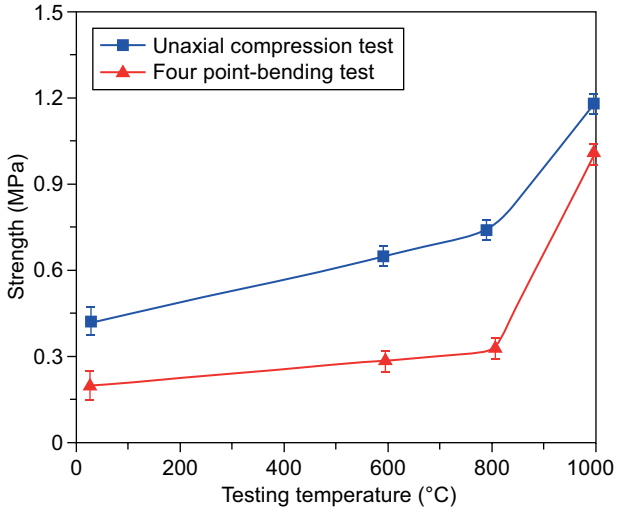

a)

Figure 4. Mechanical properties of the refractory concrete with the different testing temperatures: a) compressive and bending strength; b) axial and bending strain.

Fem simulation and results

Simulation setup

2D numerical simulations were performed to investigate the damage evolution in the refractory concrete samples subjected to a four-point bending test using CAST3M software. The sample geometry, finite element mesh, and boundary conditions are shown in Figure 5. The sample is modelled as a simply supported beam measuring 150 mm in length, with a square cross-section of 30 mm on a side and a span length of 110 mm. Quadratic quadrangular elements (QUA4) have been set for the half-sample to generate a mesh with 2250 elements and 2356 nodes, respectively.

The solution of the problem requires initial and boundary conditions. The initial conditions are given as follows:

$$T(\omega, 0) = T_0 \text{ and } T_0 \in [25, 600, 800 \text{ and } 1000\ ^\circ\text{C}]$$

$$D(\omega, 0) = 0.$$

where ω is the finite element domain, D is the isotropic damage variable and T is the temperature.

Then, a displacement is imposed at a point (P7) of the top face of the beam, Figure 5. The boundary conditions are given as follows:

$$U_x(\text{L2}, t) = 0$$

$$U_y(\text{P1}, t) = 0$$

$$U_y(\text{P7}, t) = \text{U}$$

$$T(\omega, t) = T_0$$

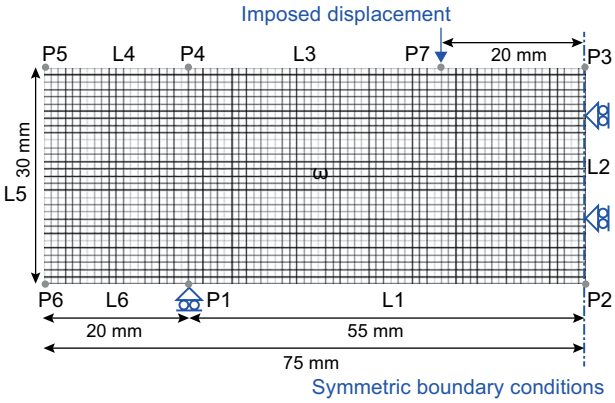

Figure 5. Illustration of the sample geometry, the finite element mesh and the boundary conditions during the four-point bending test.

Predicted damage patterns

Figure 6 shows the failure mechanisms of the half beams subjected to the four-point bending test based on the numerical simulations and experimental tests. According to the legend in Figure 6, the scale from blue to red indicates that the damage is getting worse. The damage states are influenced by the testing temperatures and are not uniformly distributed over the half beam. More precisely, Figure 6 suggests two predominant failure modes of the refractory concrete beams under an ultimate load. The first mode can be noticed in Figures 6a-c, where the red area indicates that the elements are destroyed, forming a continuous flexural crack. This type of crack can only correspond to brittle behaviour. The same results have been obtained in the experimental test, as shown in Figure 5e. However, a second failure mode can be noticed in Figure 6d, where the red area and the areas of different colours indicate that the elements are entirely and partially destroyed, respectively. According to Figure 6d, these areas form multi-localised flexural cracks and are detected as a cracked zone. Additionally, the final damaged surface obtained numerically (Figure 6d) is very similar, both in shape and size, to the damaged surface observed experimentally (Figure 5f). The tensile damage is more concentrated in the middle of the beam.

The tensile stress-strain curves predicted by the numerical simulation are compared in Figure 7 with the experimental data for the different testing temperatures: 25, 600, 800, and 1000 °C. As seen in Figure 7, the stress-strain curves indicate the quasi-brittle behaviour for the temperatures ranging from 25 to 800 °C, and these curves are almost linear up to the maximum stress. When the test temperature reaches 1000 °C, the material is viscoplastic. The current numerical simulations successfully predict the tension stress of the refractory concrete for the different testing temperatures.

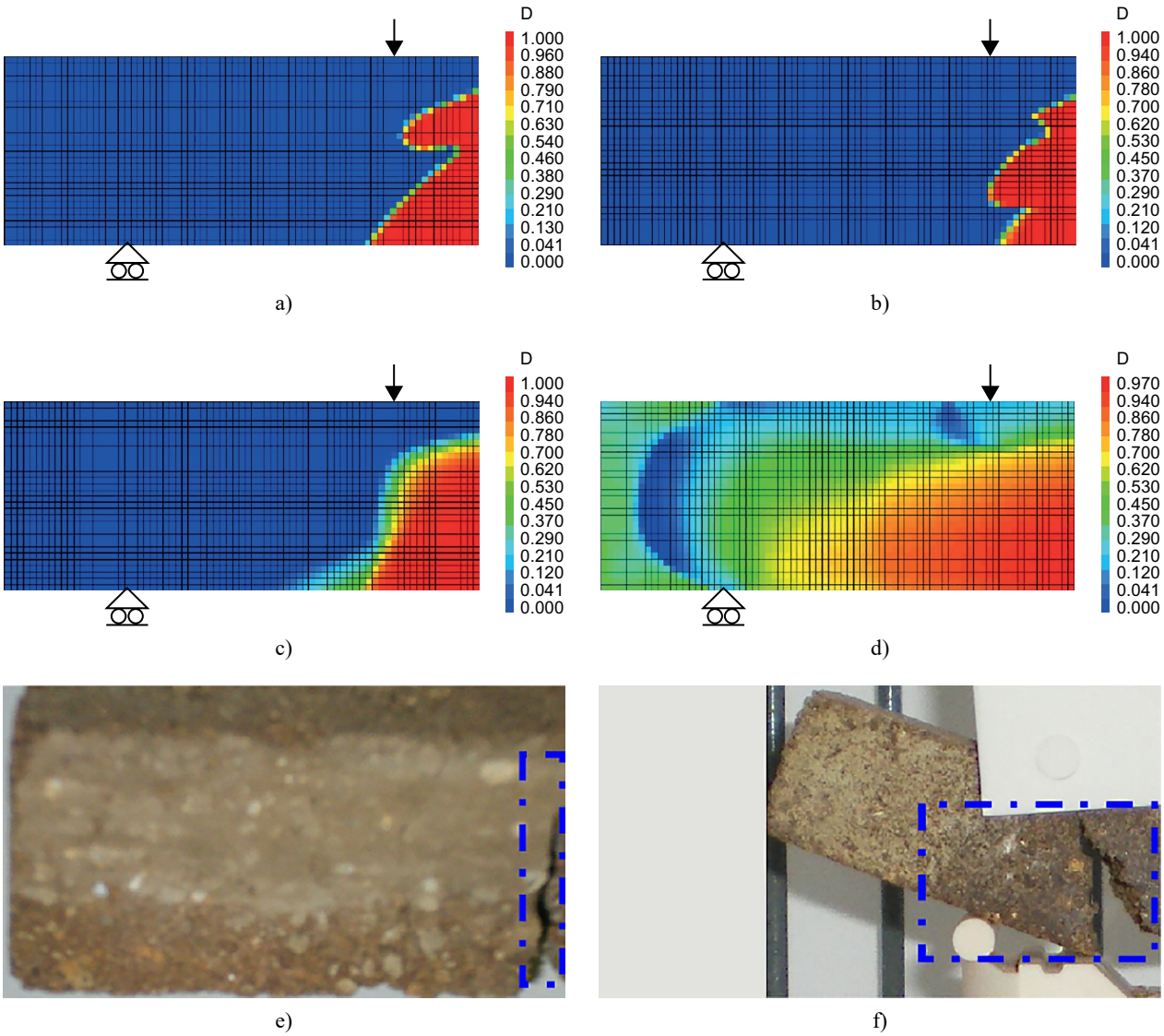

Figure 6. Numerical failure mechanisms of the samples subjected to the four-point bending tests: a) 25 °C; b) 600 °C; c) 800 °C; d) 1000 °C; e-f) damage state observed respectively at 25 °C and 1000 °C.

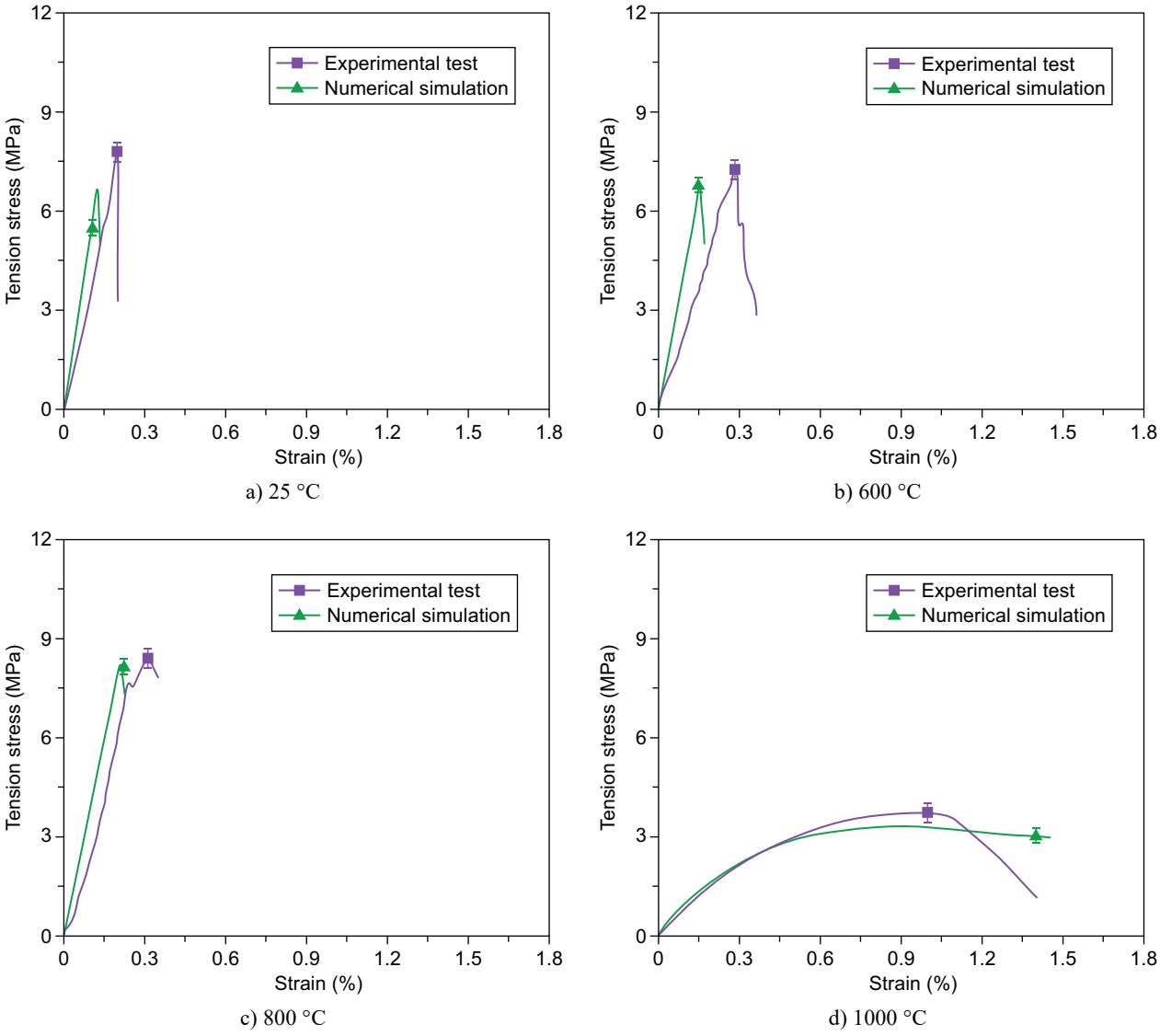

Figure 7. Comparison of the numerical and experimental bending stress-strain curves: a) 25 °C; b) 600 °C; c) 800 °C; d) 1000 °C.

Damage evolution

To better understand how damage propagates, the damage evolution process for 25 and 1000 °C of the half-sample is shown in Figures 8a and 8b, respectively. At 25 °C, a continuous flexural crack is suddenly formed as the applied vertical displacement reached 0.12 mm, indicating a brittle failure mode. At 1000 °C, the damage evolution process starts with a cracked zone in the maximum moment region at 0.05 mm. A localised damaged zone is gradually observed at this temperature and becomes larger as the applied vertical displacement increases. Consequently, this damage evolution process

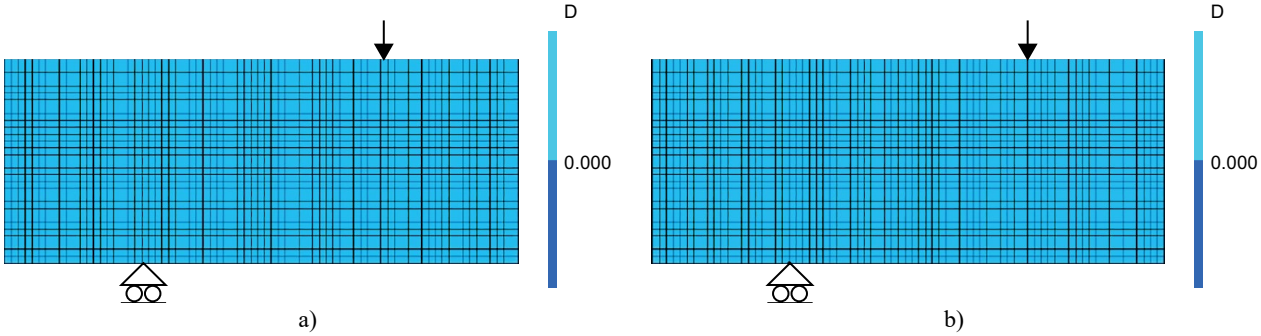

Figure 8. Damage evolution process in the half sample as the applied vertical displacement increases: a) 25 °C; b) 1000 °C.
(Continue on next page)

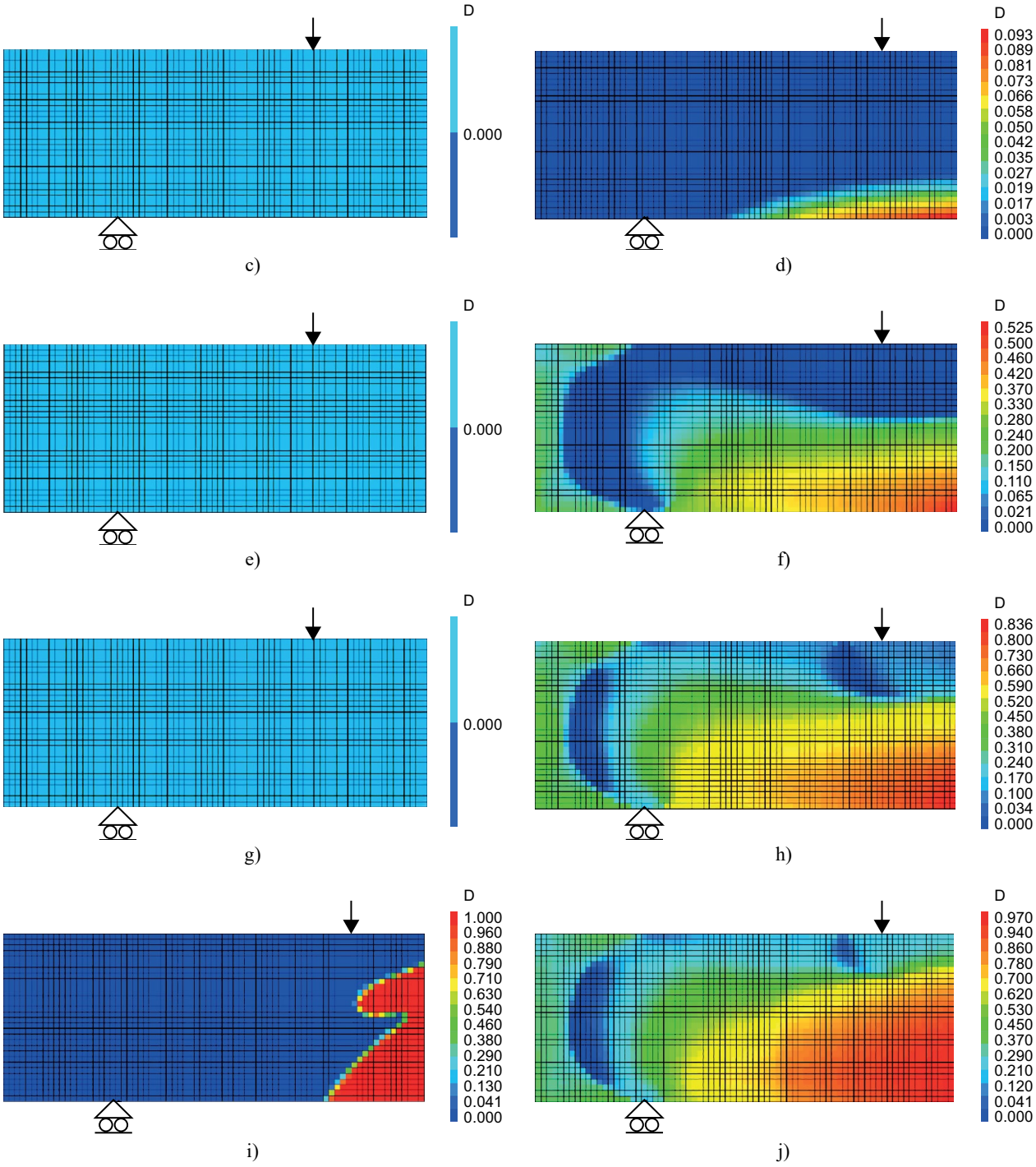

Figure 8. Damage evolution process in the half sample as the applied vertical displacement increases: a) 25 °C; b) 1000 °C.

confirms the presence of a ductile failure mode. In short, the identified model produces a realistic simulation of the experimental failure mechanisms.

Figure 9 presents the damage variable-deflection curve of the four-point bending test simulations using two different testing temperatures (25 and 1000 °C). By increasing the deflection, the damage value generally increases until cracking. The more the testing temperature increases, the more the damage variable shifts to lower values. For example, the sample tested at 1000 °C requires a deflection of 0.2 mm to achieve 0.3 (30 % damaged). In contrast, the damage variable achieves 1.0 (100 % in damage) for the sample tested at 25 °C with the same imposed displacement (0.2 mm), see Figure 9. These fast and slow damage evolutions for the testing temperatures of 25 and 1000 °C confirm the brittle and viscoplastic behaviour, respectively.

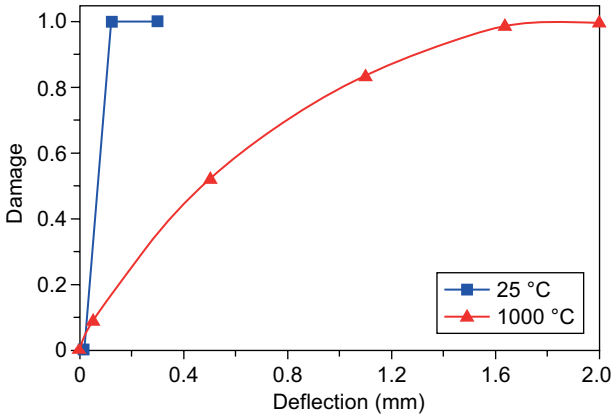

Figure 9. Evolution of the damage using the two different testing temperature: 25 and 1000 °C.

CONCLUSION

This paper experimentally and numerically investigates the thermomechanical responses and failure behaviour of refractory concrete. On the one hand, an experimental programme has been conducted to analyse the temperature effect on the behaviour of the refractory concrete samples submitted to uniaxial compression and four-point bending tests. On the other hand, an enhanced model is implemented and calibrated to simulate damage evolution within the samples at different temperatures. In addition, the model parameters are identified from the uniaxial compression and four-point bending tests using the inverse estimation approach.

The experimental investigations indicate that with an increase in the testing temperature, the thermomechanical behaviour of the refractory concrete shows a critical temperature of 800 °C, for which the compression and tensile strengths are largest. At this temperature, the amorphous phase viscosity is enough to form bridges between the different grains. Therefore, this grain bridging process generates an increase in the mechanical properties.

Similarly, the present simulations provide two kinds of failures visible on all the tested samples: a continuous crack when the testing temperature varies between 25 and 800 °C and multi-identified cracks producing a localised damage zone at 1000 °C. At this temperature, the localised damaged zone in the maximum moment region is gradually observed and becomes larger as the bending loading increases. Finally, the enhanced non-local damage model produces a realistic simulation of the experimental failure mechanisms, proving validity of the implementation method.

Acknowledgments

The work presented in this paper has been supported by Abbès Laghrour University (Khenchela, Algeria), Emergent Materials Research Unit (Sétif, Algeria), and INSA (Lyon, France). Their support is gratefully acknowledged. Also, the ICOSI laboratory is acknowledged for the technical assistance provided during the writing of this research.

REFERENCES

1. Simonin F., Olagnon C., Maximilien S., Fantozzi G. (2002): Room temperature quasi-brittle behaviour of an aluminous refractory concrete after firing. *Journal of the European Ceramic Society, 22*(2), 165–172. doi: 10.1016/s0955-2219(01)00257-6
2. Kakroudi M.G., Yeugo-Fogaing E., Gault C., Huger, M., Chotard T. (2008): Effect of thermal treatment on damage mechanical behaviour of refractory castables: Comparison between bauxite and andalusite aggregates. *Journal of the European Ceramic Society, 28*(13), 2471-2478. doi: 10.1016/j.jeurceramsoc.2008.03.048
3. Ouedraogo E., Roosefid M., Prompt N., Deteuf C. (2011): Refractory concretes uniaxial compression behaviour under high temperature testing conditions. *Journal of the European Ceramic Society, 31*(15), 2763–2774. doi: 10.1016/j.jeurceramsoc.2011.07.017
4. Martinovic S., Vlahovic M., Boljanac T., Dojcinovic M., Volkov-Husovic T. (2012): Cavitation resistance of refractory concrete: Influence of sintering temperature. *Journal of the European Ceramic Society, 33*(1), 7–14. doi: 10.1016/j.jeurceramsoc.2012.08.004
5. Benali F., Hamidouche M., Belhouchet H., Bouaouadja N., Fantozzi G. (2016): Thermo-mechanical characterization of a silica-alumina refractory concrete based on calcined algerian kaolin. *Ceramics International, 42*(8), 9703–9711. doi: 10.1016/j.ceramint.2016.03.059
6. Nader, K. (2019): Reasons for crack propagation and strength loss in refractory castables based on changes in their chemical compositions and micromorphologies with heating: special focus on the large blocks. *Journal of Asian Ceramic Societies, 7(*2), 109-126. doi: 10.1080/21870764.2019. 1597957
7. Prompt N., Ouedraogo E. (2008): High temperature mechanical characterisation of an alumina refractory concrete for Blast Furnace main trough. *Journal of the European Ceramic Society, 28*(15), 2859–2865. doi:10.1016/j.jeurceramsoc. 2008.04.031
8. Bareiro W.G., Elisa D.S., de Andrade Silva F. (2020): Numerical modeling of the thermo-mechanical behavior of refractory concrete lining. *Magazine of Concrete Research, 70*(7), 1–34. doi: 10.1680/jmacr.19.00371
9. Schmitt N., Berthaud Y., Poirier J (2000): Tensile behaviour of magnesia carbon refractories. *Journal of the European Ceramic Society, 20*(12), 2239–2248. doi: 10.1016/s0955-2219(00)00088-1
10. Simonin F., Olagnon C., Maximilien S., Fantozzi G. (2002): Room temperature quasi-brittle behaviour of an aluminous refractory concrete after firing. *Journal of the European Ceramic Society, 22*(2), 165–172. doi:10.1016/s0955-2219(01)00257-6
11. Baghdadi M., Dimia S.M., Guenfoud M., Bouchair A. (2021): An experimental and numerical analysis of concrete walls exposed to fire. *Structural Engineering and Mechanics, 77*(1), 819-830. doi: 10.12989/sem.2021.77.6.819

12. Aksel C. (2002): The role of fine alumina and mullite particles on the thermomechanical behaviour of alumina-mullite refractory materials. *Materials Letters, 57*(3), 708–714. doi: 10.1016/s0167-577x(02)00858-3
13. Boussuge M. (2008): Investigation of the thermomechanical properties of industrial refractories: the French programme PROMETHEREF. *Journal of Materials Science, 43*(12), 4069–4078. doi: 10.1007/s10853-008-2534-0
14. Amrane B., Ouedraogo E., Mamen B., Djaknoun S., Mesrati N. (2011): Experimental study of the thermo-mechanical behaviour of alumina-silicate refractory materials based on a mixture of Algerian kaolinitic clays. *Ceramics International, 37*(8), 3217–3227. doi: 10.1016/j.ceramint.2011.05.095
15. Grassl P., Xenos D., Nyström U., Rempling R., Gylltoft K. (2013): CDPM2 A damage-plasticity approach to modelling the failure of concrete. *International Journal of Solids and Structures, 50*(24), 3805-3816. doi: 10.1016/j.ijsolstr.2013.07.008
16. Juárez-Luna G., Méndez-Martínez H., Ruiz-Sandoval M.E. (2014): An isotropic damage model to simulate collapse in reinforced concrete elements. *Latin American Journal of Solids and Structures, 11(*13), 2444-2459. doi: 10.1590/S1679-78252014001300007
17. Pelà L., Cervera M., Roca P. (2013): An orthotropic damage model for the analysis of masonry structures. *Construction and Building Materials, 41*, 957-967. doi: 10.1016/j.conbuildmat.2012.07.014
18. Wang Z., Jin X., Jin N., Shah A.A., Li B. (2014): Damage based constitutive model for predicting the performance degradation of concrete. *Latin American Journal of Solids and Structures, 11*(6), 907-924. doi: 10.1590/S1679-78252014000600001
19. Maimí P., Camanho P.P., Mayugo J.A., Dávila C.G. (2007): A continuum damage model for composite laminates: Part I–Constitutive model. *Mechanics of Materials, 39(*10), 897-908. doi: 10.1016/j.mechmat.2007.03.005
20. Mazars J., Hamon F., & Grange S. (2014): A new 3D damage model for concrete under monotonic, cyclic and dynamic loadings. *Materials and Structures, 48*(11), 3779-3793. doi: 10.1617/s11527-014-0439-8
21. Paredes J.A., Oller S., Barbat A.H. (2016): New Tension-Compression Damage Model for Complex Analysis of Concrete Structures. *Journal of Engineering Mechanics, 142(*10), 04016072. doi:10.1061/(ASCE)EM.1943-7889.0001130
22. Djaknoun S., Ouedraogo E., Ahmed Benyahia A. (2013). Numerical analysis of the behaviour of notched specimens at various testing temperatures using an elastic damage model, In: *8th International Conference on Fracture Mechanics of Concrete and concrete Structures (FraMCoS)*, Toledo, Spain, March. 10-14, pp.1528-1538. https://framcos.org/FraMCoS-8/p485.pdf
23. Mamen B., Kolli M., Ouedraogo E., Hamidouche M., Djoudi H., Fanttozi G. (2018): Experimental characterisation and numerical simulation of the thermomechanical damage behaviour of kaolinitic refractory materials. *Journal of the Australian Ceramic Society, 55*, 555-565. doi: 10.1007/s41779-018-0262-8
24. Kolli M., Hamidouche M., Bouaouadja N., Fantozzi G. (2012): Thermomechanical characterization of a fire clay refractory made of Algerian Kaolin. *Annales de Chimie Science des Matériaux, 37,* 71-84. doi: 10.3166/acsm.37.71-84
25. ASTM C860-15, "Standard Test Method for Determining the Consistency of Refractory Castable Using the Ball-In-Hand Test", ASTM International, West Conshohocken, PA, 2019. doi: 10.1520/C0860-15R19
26. Giry C., Dufour F., Mazars J. (2011): Stress-based nonlocal damage model. *International Journal of Solids and Structures, 48*(25-26), 3431–3443. doi: 10.1016/j.ijsolstr.2011.08.012
27. Pijaudier-Cabot G., Bažant Z.P. (1987): Nonlocal damage theory. *Journal of Engineering Mechanics, 113*(10), 1512–1533. doi: 10.1061/(asce)0733-9399(1987)113:10(1512)
28. Mazars J. (1984). *Application de la mécanique de l'endommagement au comportement non linéaire et à la rupture du béton de structure*. Doctorat Es-Sciences Physiques, Université Paris VI. https://www.worldcat.org/title/application-de-la-mecanique-de-lendommagement-au-comportement-non-lineaire-et-a-la-rupture-du-beton-de-structure/oclc/490668452